Numerical models of flow patterns around a rigid inclusion in a viscous matrix undergoing simple shear: implications of model parameters and boundary conditions

Nibir Mandal[a], Susanta Kumar Samanta[a], Chandan Chakraborty[b,*]

[a]Department of Geological Sciences, Jadavpur University, Kolkata 700032, India
[b]Geological Studies Unit, Indian Statistical Institute, 203, B.T. Road, Kolkata 700108, India

Abstract

The hydrodynamic models that have recently been developed to investigate the nature of flow around coherent, rigid inclusions in simple shear reveal two contrasting patterns with eye-shaped and bow-tie shaped separatrix, even though all the models are based on Navier–Stokes law. In order to find the cause of this variance, this paper reviews the existing models in the light of different boundary conditions imposed on individual models. Scrutiny of the models reveals that inclusion–matrix systems, when considered infinitely extended in space, develop eye-shaped flows. However, those with finite dimensions essentially display bow-tie shaped flows. Using a finite element method (FEM), we advance the study to show the additional effects of model/inclusion dimension ratio (D_R) and model aspect ratio (A_R) under different boundary conditions. In the flow with bow-tie shaped separatrix, the regions of back flow define a nearly semi-circular geometry when D_R is low (<2). These regions assume a semi-elliptical shape with increasing D_R. The distance of stagnation points from the inclusion is found to increase non-linearly with D_R. Model results suggest that transformation of a flow with eye-shaped separatrix to that with bow-tie shaped separatrix can occur due to increasing A_R under a specific boundary condition. Applying FEM results in geological situations thus requires the appropriate choice of dimensional parameters of the model as well as the kinematic conditions imposed at the model boundaries.

1. Introduction

Under simple shear deformation, the presence of circular rigid inclusions within a ductile matrix induces perturbations in the flow, which results in two major flow types: one with eye-shaped separatrix and the other with bow-tie shaped separatrix (Fig. 1; cf. Passchier and Soukoutis, 1993; Passchier et al., 1993; Passchier, 1994; Bons et al., 1997). Physical and numerical experiments suggest that the geometry of porphyroclast tails (e.g. ϕ-, σ-, δ-types) is primarily controlled by the nature of flow around inclusions (Passchier and Simpson, 1986; Passchier and Soukoutis, 1993; Passchier et al., 1993; Passchier, 1994; Bons et al.,

* Corresponding author.
  E-mail address: chandan@isical.ac.in (C. Chakraborty).

1997; Mandal et al., 2000; Bose and Marques, 2004). Accordingly, there have been several attempts to investigate the different physical parameters that could control the flow pattern (Masuda and Ando, 1988; Bjornerud and Zhang, 1995; ten Brink and Passchier, 1995; Masuda and Mizuno, 1996; Jezek et al., 1999; Pennacchioni et al., 2000; Mandal et al., 2001; Marques and Coelho, 2001; Taborda et al., 2004; Marques et al., 2005). Matrix rheology (Passchier, 1994) and inclusion–matrix coherence (Pennacchioni et al., 2000) have been identified as possible factors influencing the flow pattern. Samanta et al. (2003) have shown that the flow pattern changes from eye-shaped to bow-tie shaped with increase in volume concentration of inclusion in a multiple inclusion system. Using FEMs Marques et al. (2005) derived a variety of flow paths by varying the ratio of shear-model width and inclusion diameter (S). Employing very small values of this ratio (1.1–1.5) they have obtained flow patterns, which do not conform to any of the previous results. For example, their simulations yield multiple
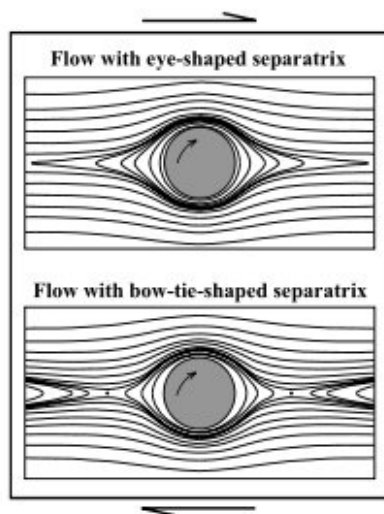
Fig. 1. Two principal types of flow around a circular rigid inclusion under simple shear: flow with eye-shaped separatrix and flow with bow-tie shaped separatrix.

stagnation points in the flow. However, this type of flow field is yet to be verified from physical experiments and explored in relation to geological features, such as porphyroclast tails, commonly observed in natural shear zones.

It follows from the above discussion that the flow pattern around a rigid inclusion may show a wide variation depending on the modeling approach and choice of boundary conditions (Bons et al., 1997). In this paper, we thus review the existing continuum models, and from there deduce the physical basis for the development of eye-shaped and bow-tie shaped flow pattern in a single-inclusion/matrix system under natural conditions. The study is advanced to demonstrate the effects of matrix:inclusion volume proportion, model geometry and boundary settings on the nature of flow around a circular, coherent inclusion.

2. Review of continuum models

In this discussion we consider only those models that describe the flow patterns around circular, coherent rigid inclusions under bulk shear flow. With the help of an analytical solution of the velocity functions, based on Navier–Stokes equations, Masuda and Ando (1988) determined particle paths around a rigid inclusion. The expressions of the velocity functions were derived for a model with the following kinematic conditions at the model boundaries (Fig. 2a)

$$u = 1, \ v = 0, \ w = 0 \text{ at } z = 5 \tag{1a}$$

$$u = -1, \ v = 0, \ w = 0 \text{ at } z = -5 \tag{1b}$$

where u, v, w are velocity components along the Cartesian co-ordinate axes, x, y and z, respectively, and the model is considered as being deformed by shear $\gamma = 1$ along x-axis on

the xz plane. Considering that the inclusion rotates at an angular speed of half the bulk shear rate (Jeffery, 1922; Ghosh and Ramberg, 1976; Passchier, 1986), the velocity conditions at the inclusion–matrix interface can be given by

$$u = -z/10, \ v = 0 \text{ and } w = x/10 \text{ at } r = 1 \tag{2}$$

where r is the inclusion radius. Based on the solid harmonic functions (Lamb, 1932) they have determined the velocity field around a fixed inclusion, and then added it with that of a rotating inclusion, the expression of which is as follows:

$$u_{\mathrm{b}} = -\frac{z}{10r^3}, \quad v_{\mathrm{b}} = 0, \quad w_{\mathrm{b}} = \frac{x}{10r^3} \tag{3}$$

The values of the velocity components becomes negligibly small at the model boundaries ($z = \pm 5$), and so Masuda and Ando (1988) assumed that the flow perturbations due to rotation of rigid inclusion vanishes at the model boundary. Following this theoretical approach they obtained particle paths around a rigid inclusion under bulk shear, which is characterized by eye-shaped separatrix (Fig. 2a). In this flow there is no stagnation points defining the boundary of flow reversal on the central plane parallel to the bulk shear plane, which is also evident from Eq. (3) representing the perturbations by the rigid rotation of inclusions. The perturbations due to a stationary inclusion in simple shear flow do not contribute to motion of particles across the shear-parallel central plane (see eqs. (4) and (5) of Masuda and Ando (1988)).

ten Brink and Passchier (1995) presented results obtained from computer simulations, demonstrating the streamline patterns around a circular rigid body. A rectangular (aspect ratio: 3) model was chosen for the simulation, where its width is 1.5 times the inclusion diameter. It appears that the deformation conditions at the model boundaries were set similar to that occurring in ring shear (see Bons et al., 1997). In this case the shear profile at the lateral boundaries of the model may deviate from that of homogeneous simple shear. In contrast to the model of Masuda and Ando (1988), their model develops a flow pattern with bow-tie shaped separatrix (Fig. 2b). The stagnation points are located at a distance of nearly 0.5 times the inclusion radius. The width of the hyperbolic separatrix occurring between uni-directional and reversing flow paths attains a maximum value of about 0.5 the inclusion radius (Fig. 2b).

Employing the FEM, Masuda and Mizuno (1996) studied the flow patterns around circular rigid inclusions considering both Newtonian and non-Newtonian matrices. They considered finite models with length and width 2.68 times the inclusion diameter. A Cartesian co-ordinate reference, xy, is chosen at the inclusion center with the x-axis parallel to shear direction. The boundary conditions for the velocity components follow:

At the model boundary,

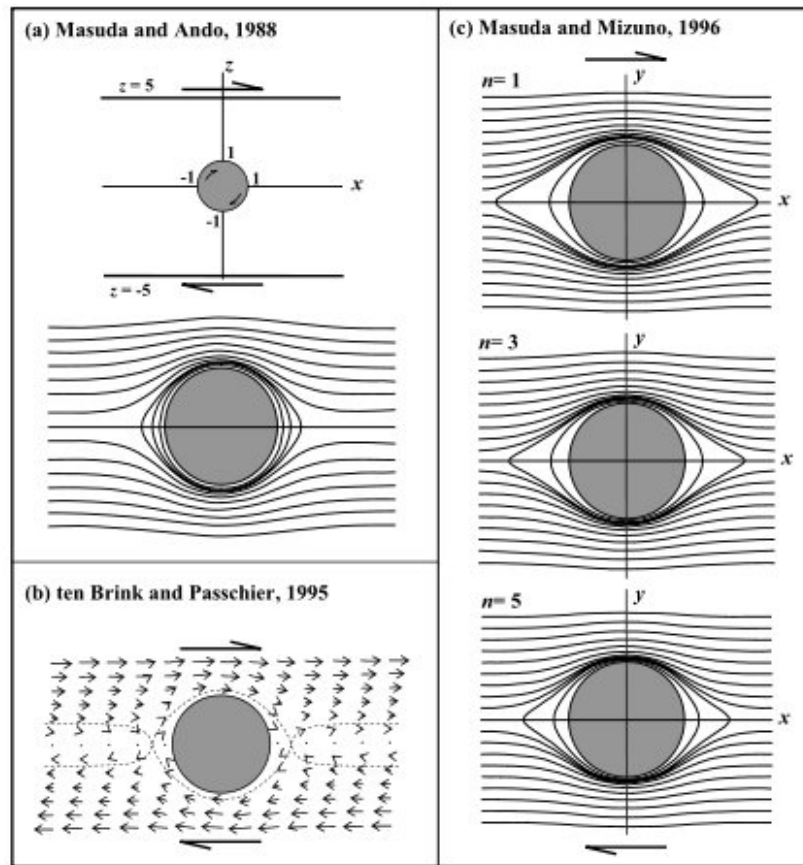$$u = y \text{ and } v = 0, \text{ (taking far} - \text{field shear strain rate } \gamma = 1) \tag{4}$$

Fig. 2. (a) Flow around a rigid inclusion in numerical model under simple shear (after Masuda and Ando, 1988). Initial model with geometrical considerations (above) and particle paths with eye-shaped separatrix (below). (b) Numerical simulation of displacement vectors (arrows) in flow around a circular rigid inclusion under dextral shear (after ten Brink and Passchier, 1995). Note bow-tie shaped separatrix (dashed lines) in the flow. The initial model was rectangular, and deformed by giving shear displacements at the upper and lower boundaries, simulating the condition as in ring shear. (c) Eye-shaped flow patterns in models with matrix of power-rheology (after Masuda and Mizuno, 1996). *n*, stress exponent. Note that the flow pattern does not change significantly with increasing *n*.

At the surface of inclusion,

$$u = wy \text{ and } v = -wx \tag{5}$$

u and v are velocity components along the x- and y-axis, respectively. They have shown that w, rotation rate of spherical inclusion, will be 0.5γ, irrespective of matrix rheology. In the FEMs there were 504 triangular elements with 36 nodes on the periphery of the area and on the periphery of inclusion. In each triangular element, the velocity components were expressed in terms of linear functions as

$$u = a + bx + cy \tag{6a}$$

$$v = d + ex + fy \tag{6b}$$

a, b, c… are unique constants for each triangular element, which need to be determined employing FEMs (details given in Masuda and Mizuno (1996)). Models with $n=1$ develop particle paths with an eye-shaped separatrix (Fig. 2c), which is reasonably consistent with that of Masuda and Ando (1988). Models with $n>1$ show similar flow patterns around rigid inclusions, albeit there are some quantitative changes in the flow with increasing n. In models

with $n=3$, particles located at a distance of $1.07R$ (R: inclusion radius) show close paths intersecting the central line parallel to the shear direction at a distance of $2.03R$. On the other hand, for $n=5$, a particle at a distance of $1.05R$ describes a close path intersecting the central line at a distance of $1.77R$. However, the overall pattern of particle paths does not vary dramatically with increasing n, i.e. non-linearity in matrix rheology. According to the FEMs of Masuda and Mizuno (1996) the flow pattern around a rigid sphere is characterized by eye-shaped separatrix, irrespective of matrix rheology, in contrast to the model of ten Brink and Passchier (1995) demonstrating the flow pattern with bow-tie shaped separatrix. They infer, with the help of an analytical solution for the flow field (eq. (25) of Masuda and Mizuno, 1996), that there cannot be any stagnation points even if the model is considered large in its lateral extent.

Pennacchioni et al. (2000) investigated the nature of flow around a circular rigid inclusion in FEMs for both Newtonian and non-Newtonian rheology of the matrix. The models have been developed considering Navier–Stokes equations:

$$\mu\nabla^2 u - \nabla p = 0 \tag{7a}$$

and the equation of continuity:

$$\nabla u = 0 \tag{7b}$$

They have employed FEMs in two dimensions. The models are based on the first quadrant of the Cartesian space considered at the center of inclusion, taking into account a square region with the side length five times the inclusion radius (Fig. 3a). The region is meshed including 2204 quadrilateral elements and 2108 nodes. In the present discussion we consider their models containing coherent inclusions, which rotate with a velocity half the bulk shear rate. Their models always yield streamline patterns with bow-tie shaped separatrix (Fig. 3a). The streamline patterns do not vary significantly with increasing value of stress exponent (n). Flow with eye-shaped separatrix develops only when a slip condition is imposed at the inclusion–matrix interface. It thus appears that the results of Masuda and Mizuno (1996) and Pennacchioni et al. (2000) do not converge, even though both the analyses deal with power law rheology of the matrix.

Mandal et al. (2001) have shown the flow pattern around a rigid inclusion embedded in an infinitely extended viscous medium. Based on Jeffery's theory, they have described velocity functions for flow around an elliptical inclusion. Considering the bulk deformation in simple shear, the expressions of the functions follow:

$$u = \frac{\dot{\gamma}_b}{2}\left[2(\alpha D - \beta C) + E\gamma\right]y + \dot{\gamma}_b y$$

$$- \frac{2\Delta xy}{b'^2 x^2 + a'^2 y^2}\left[\frac{\dot{\gamma}_b}{2}\left\{\frac{E + 2a'^2 C + 2b'^2 D}{a'^2}\right\}x\right] \tag{8a}$$

$$v' = -\frac{\dot{\gamma}_b}{2}\left[2(\alpha D - \beta C) - E\gamma\right]x$$

$$- \frac{2\Delta xy}{b'^2 x^2 + a'^2 y^2}\left[\frac{\dot{\gamma}_b}{2}\left\{\frac{E + 2a'^2 C + 2b'^2 D}{b'^2}\right\}y\right] \tag{8b}$$

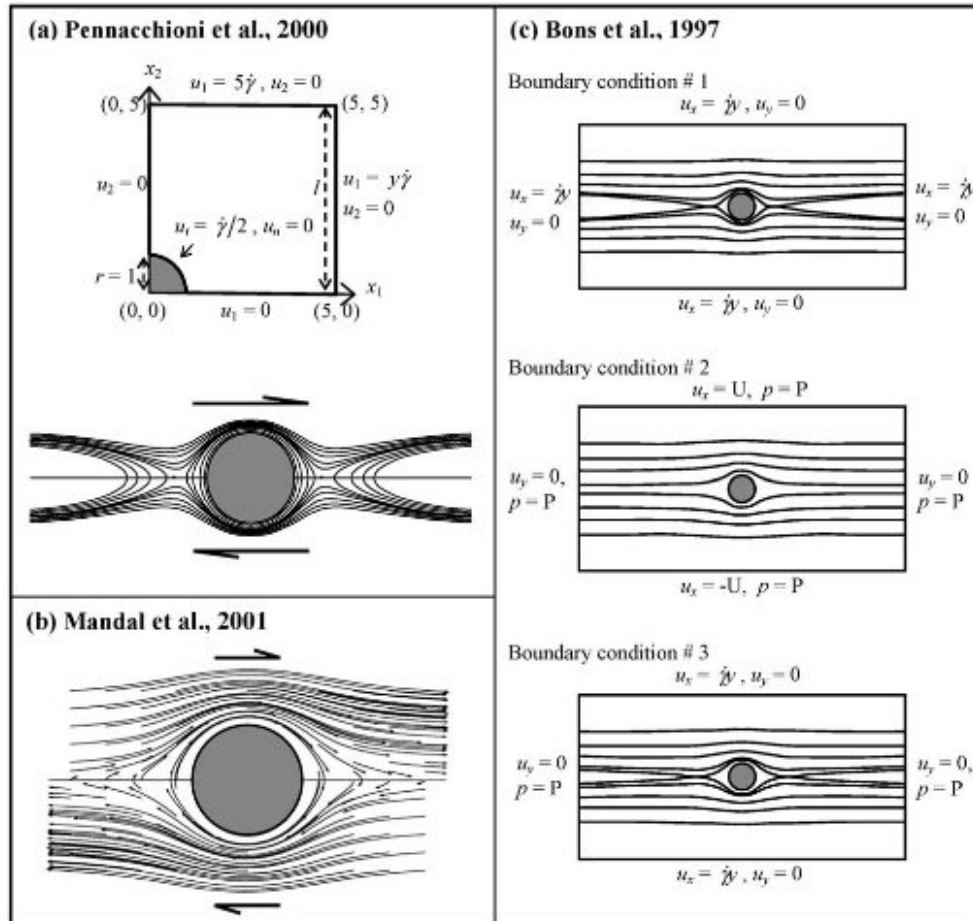where $a' = \sqrt{a^2 + \lambda}$, $b' = \sqrt{b^2 + \lambda}$ and $\Delta = a'b'$. The

Fig. 3. (a) Consideration of a quarter finite element model (above) by Pennacchioni et al. (2000). Radius of inclusion, $r = 1$. u_1 and u_2 are velocity components along x_1 and x_1 axes of the Cartesian coordinate axes chosen at the center of inclusion. u_t and u_n are tangential and normal velocity components, respectively, at the boundary of inclusion, which rotates at an angular velocity of $\dot{\gamma}/2$, $\dot{\gamma}$ is the rate of bulk shear. Displacement conditions are shown in terms of u_1 and u_2 at the model boundaries. Corresponding flow pattern (bow-tie shaped) is shown below. Solid circles mark stagnation points. (b) Particle paths in numerical model run based on a velocity function for an infinitely extended matrix (Mandal et al., 2001). (c) Streamline patterns in models of Bons et al. (1997) under three boundary conditions shown in terms of velocity components parallel and perpendicular to the shear direction, u_x and u_y and pressure p. P is the constant background pressure.

parameters in Eqs. (8a) and (8b) have the following expressions:

$$\alpha = \frac{2}{(a^2 - b^2)} \left[\frac{a' - b'}{a'} \right], \quad \beta = \frac{2}{(a^2 - b^2)} \left[\frac{a' - b'}{b'} \right],$$

$$\gamma = \frac{2}{(a^2 - b^2)^2} \left[\frac{(a' - b')^2}{a'b'} \right]. \quad A = \frac{(a + b)^2}{8},$$

$$B = -\frac{(a + b)^2}{8}, \quad C = D = \frac{ab(a + b)^2}{4(a^2 + b^2)},$$

$$E = -ab \frac{(a + b)^2}{2}, \quad F = \frac{a^2 + b^2}{4}(a + b)^2$$

With the help of the velocity functions (Eqs. (8a) and (8b)) they have simulated the flow around a rigid inclusion in simple shear (Fig. 3b). The flow pattern is characterized by eye-shaped separatrix, which is similar to that shown by Masuda and Ando (1988). In Eq. (8b) the velocity component at right angle to the shear direction cannot be zero on the shear-parallel central plane (i.e. $y = 0$) for $x > 0$. It is thus possible to infer analytically that a circular inclusion embedded in an infinitely extended matrix, subjected to a far-field homogeneous shear, cannot have any stagnation points, which are required for the flow with bow-tie shaped separatrix. This can be shown analytically again using Lamb's theory. Using the theory, Happel (1957) derived the velocity functions of flow around rigid inclusions as a function of volume concentration of inclusions. In the case of very low concentrations, the expressions in polar coordinates can be written as:

$$v_r = \frac{1}{2} \left[1 - \frac{5}{2} \left(\frac{a}{r} \right)^3 + \frac{3}{2} \left(\frac{a}{r} \right)^5 \right] \dot{\gamma} r \sin 2\theta \qquad (9a)$$

$$v_\theta = \frac{1}{2} \left[1 - \left(\frac{a}{r} \right)^5 \right] \dot{\gamma} r \cos 2\theta - \frac{\dot{\gamma}}{2} r \qquad (9b)$$

where a is the radius of inclusion. The last term in Eq. (9b) represents the rigid rotation component of bulk shear. According to Eq. (9b), the velocity of particles across the central line parallel to the shear direction ($\theta = 0$) cannot be zero for any finite value of r, which is required to define the stagnation points in a flow with bow-tie shaped separatrix. It thus appears from Happel's analysis also that the flow around a circular inclusion will be essentially characterized by eye-shaped separatrix.

The work of Bons et al. (1997) demonstrates that the contrasting flow patterns develop due to differences in the boundary conditions imposed on the models. They have considered square initial models, containing an inclusion with a diameter 1/12th the model dimension, and effective viscosity 100 times that of the matrix. Two parameters were considered at the boundary: background pressure and velocity vectors, which can be independently set at the boundaries of FEMs. The three conditions are as follows (Fig. 3c): (1) the model is deformed by homogeneous shear displacement at its four boundaries as is done in shear box

experiments. (2) The model involves shear-parallel displacement component at the model boundaries parallel to the bulk shear, and no shear-across velocity component at the other pair of model boundaries, and imposes a constant background pressure acting as normal stress to all the model boundaries. This simulates an inclusion–matrix system where simple shear boundary conditions are imposed at infinity from the inclusion. (3) The shear-parallel model boundaries are subjected to the condition as in condition 1 but the side boundaries are kept under a normal stress equal to a constant background pressure and there is no velocity across the shear direction such as in a ring shear apparatus. Bons et al. (1997) have shown that flow with eye-shaped separatrix develops only under boundary condition 2, which is considered to be the best approximate for the solution of the case of inclusion within an infinitely extended matrix. Flows with bow-tie shaped separatrix are obtained in the other two conditions (Fig. 3c).

We now attempt to understand the flow perturbations in an infinitely extended inclusion–matrix system from the physical point of view. A homogeneous, steady state shear flow can be represented by a set of parallel particle paths and streamlines in the matrix without any rigid inclusion (Fig. 4a). The presence of an inclusion in the system would perturb the flow path in the radial directions as when a spherical body is set in a stationary fluid yielding radial streamlines (Fig. 4b). Understandably, the radial perturbation would tend to be zero away from the body. The resultant of the streamlines for homogeneous flow and the perturbed one will be symmetrically distorted resulting in a convexity perpendicular to the shear direction (Fig. 4c). Now, the spherical body, if considered to be rotating in the stationary medium, would induce additional tangential flow in its neighborhood, forming concentric streamlines (Fig. 4d), as given in Eq. (3) (Masuda and Ando, 1988). This implies that all the particles lying along the shear-parallel central line will be set in motion at a right angle to the shear direction. The combination of homogeneous shear flow, radial flow and the tangential flow is likely to result in a set of closed streamlines encased with open streamlines with convexity away from the center of the body (Fig. 4e). In this construction no particles lying on the shear plane can remain stationary, defining stagnation points as in the case of flow patterns with bow-tie shaped separatrix. A spherical body floating in an infinitely extended matrix will necessarily show particle paths with eye-shaped separatrix, which is also evident from the velocity function given by Jeffery (1922) and Happel (1957). In Section 3 we attempt to explore and analyze probable factors leading to flows with stagnation points in flow and thereby separatrix with bow-tie shaped geometry.

3. Flow patterns in FEMs

3.1. Model parameters

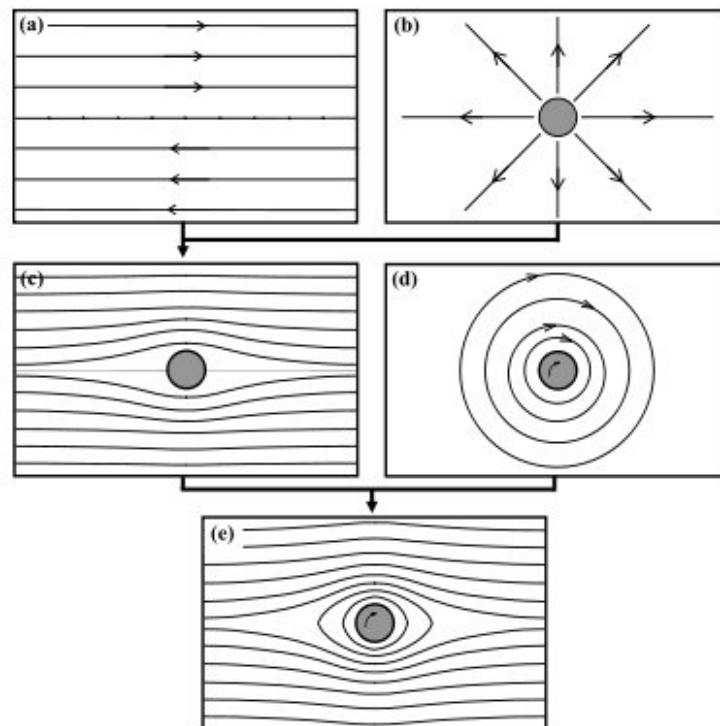We ran experiments in FEMLAB software to simulate

Fig. 4. Schematic illustrations of perturbations in shear flow due to the presence of a rigid inclusion. (a) A set of parallel lines representing streamlines of a homogeneous shear flow. (b) Radial streamlines of flow perturbations due to spatial occupation of a circular inclusion in a stationary fluid. (c) Parallel streamlines are distorted into bi-convex shapes when the perturbations in (b) are added. (d) Circular streamlines for flow induced by the rotational motion of a rigid inclusion in a stationary fluid. (e) Streamline pattern obtained by superposing the streamlines in (c) and (d) one over another.

flow patterns around a coherent, circular rigid inclusion, and investigate how the choice of model parameters can lead to variation in the nature of flow. The following parameters have been considered in the simulations: (1) model/inclusion dimension ratio (D_R), (2) aspect ratio of model (A_R), and (3) boundary settings (Fig. 5). D_R is the ratio of side length of square models and inclusion diameter, which is used as a measure of the volume proportion of the inclusion. We choose D_R to show how the flow pattern can vary depending on the volume proportion occupied by the inclusion in the model (cf. Samanta et al., 2003; Treagus and Lan, 2004). The parameter D_R and the parameter S of Marques et al. (2005) may seem to be similar. However, D_R is to be distinguished from S, as the latter is a measure of confinement of the matrix in the direction perpendicular to the bulk shear.

A_R is a parameter concerning rectangular FEMs, which is used to investigate the effect of model geometry on the flow pattern. We take A_R as the ratio of model dimensions parallel and perpendicular to the shear direction (Fig. 5a). Model experiments were run imposing any of the following three boundary settings (Fig. 5b): (a) homogeneous shear displacements, (b) unconstrained lateral boundaries, and (c) straight-out conditions. The first setting can be compared with that adopted in shear box experiments, where the model is deformed in simple shear by moving plates at its four boundaries. Evidently, this condition does not match with that in an infinitely extended inclusion–matrix system

being deformed under far-field simple shear, as the strain at any finite distance from the inclusion will be essentially heterogeneous, and will tend to be homogeneous only at infinite distances. We have considered the second condition to show the flow in models with lateral faces in an unconstrained state. In this case the lateral model boundaries are not displaced by moving any plates, as done in shear box experiments, and the flow at the edges deviates from that of homogeneous simple shear. With this condition we aim to investigate the perturbed flow around a rigid inclusion confined between two parallel rigid plates moving in opposite directions, where the setting at the lateral boundaries is given in terms of a constant pressure. In FEMLAB one can impose the straight-out condition at the side boundaries of the model, which is expressed using mathematical equations as:

$$t.u = 0 \qquad (10a)$$

$$p = 0 \qquad (10b)$$

t is the unit tangent vector to the surface under consideration. The condition given in Eq. (10a) implies that flow at the model edges takes place normal to the model boundaries, showing no tangential velocity component. The second equation (Eq. (10b)) indicates that the lateral faces of the model are free from any external pressure. The velocity profile is thus likely to deviate from that of ideal simple shear. This boundary condition is comparable with that in ring shear (cf. Bons et al., 1997).
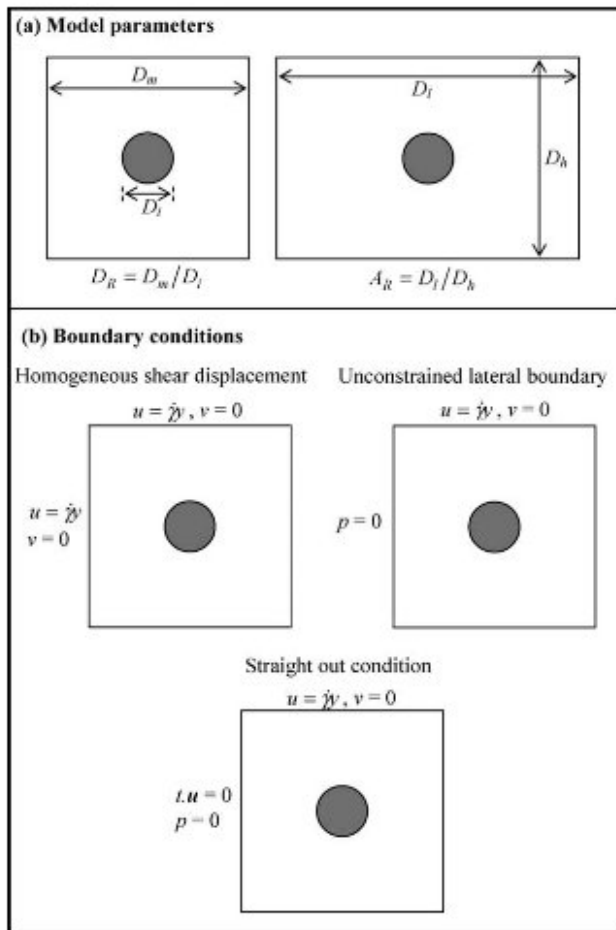
(a) Model parameters

$$D_R = D_m/D_i \qquad\qquad A_R = D_l/D_h$$

(b) Boundary conditions

Homogeneous shear displacement   Unconstrained lateral boundary

$u = \dot{\gamma}y, v = 0$ $u = \dot{\gamma}y, v = 0$

$u = \dot{\gamma}y$
$v = 0$ $p = 0$

Straight out condition

$u = \dot{\gamma}y, v = 0$

$t.u = 0$
$p = 0$

Fig. 5. (a) Definitions of model parameters: D_R is the ratio of side length square model (D_m) and inclusion diameter (D_i) and A_R is the aspect ratio of rectangular model. (b) Three boundary conditions employed in finite element models. The conditions are imposed in terms of velocity components, u and v, parallel and perpendicular to the shear direction and/or pressure $p.\dot{\gamma}$ is the rate of shear at the model boundaries.

3.2. Effects of model/inclusion dimension ratio

We ran a set of experiments on square FEMs by varying D_R employing the boundary condition (a), mentioned in Section 3.1. The velocity condition at the inclusion–matrix interface was imposed considering that the inclusion rotates at a rate half the bulk shear rate. Experimental runs show that the flow pattern strongly varies when the model to inclusion dimension ratio (D_R) is changed. For a low dimension ratio, e.g. $D_R = 2$, the streamlines are characterized by bow-tie shaped separatrix. Particles in a large part of the model away from the inclusion move across the central shear plane and reverse their movement direction (Fig. 6a). Values less than 2 (e.g. 1.2, 1.5, etc.) also yield similar patterns with the difference that the stagnation points are located closer to the inclusion. The separatrix between particles with unidirectional and reversal motion are nearly circular in shape, and its width is about one third of the model dimension. The distance of the stagnation points

from the inclusion center is 1.13 times the inclusion radius. The flow geometry is similar to those observed in systems containing inclusion in high concentrations (fig. 5 of Samanta et al., 2003). With increase in D_R both the shape of separatrix and the distances of the stagnation points vary significantly. The streamlines corresponding to particles with reverse motion become progressively narrower, assuming a semi-elliptical shape. In addition, the distance of stagnation points continuously increases with increasing D_R (Fig. 6b).

It should be mentioned that the nature of variation of the geometry of flow and location of stagnation points with D_R (Fig. 6) is markedly different from that obtained by Marques et al. (2005) by varying the parameter S (model width/inclusion diameter) (their figs. 7–9). However, it is to be noted that in our simulations we showed the effect of D_R with a constant aspect ratio of the model ($=1$). In the models of Marques et al. (2005), the value of S was varied by changing both the model width and inclusion diameter but keeping the model length constant. This implies that in their analysis the model aspect ratio changed with changing S. It thus appears that the variation in the flow pattern that they assign only to S, perhaps includes also the effect of aspect ratio of the model. In Section 3.3 we discuss how the aspect ratio can independently affect the flow keeping the inclusion diameter constant.

3.3. Effect of model aspect ratio

The flow pattern around an inclusion can change significantly depending on the aspect ratio (A_R) of the model. When A_R is low ($=0.5$), the flow shows eye-shaped separatrix (Fig. 7a). With increase in model ratio ($A_R = 1$), stagnation points appear and the flow defines a bow-tie shaped separatrix (Fig. 7b). The bow-tie shaped flow becomes more and more prominent with further increase in shear parallel model dimension (Fig. 7c). It should be noted that this variation occurs even though the model width/inclusion diameter (i.e. the S value of Marques et al., 2005) in both the models (Fig. 7b and c) is the same.

3.4. Effects of mechanical conditions at model boundaries

In this section we demonstrate that the flow pattern can be sensitive to dynamic conditions imposed at the model boundaries, leading to contrasting types of flow. Let us first consider models being deformed by simple shear. The lateral faces of the models are kept unconstrained and free of any pressure from the ambience (i.e. *boundary condition-b*). Under such a condition, particles show close paths in the model with aspect ratio 1. However, typical eye-shaped geometry occurs only in the close neighborhood of the inclusion (Fig. 8a). This boundary condition never produces flow with bow-tie shaped separatrix even when the model dimensions are reduced keeping the aspect ratio fixed at 1.
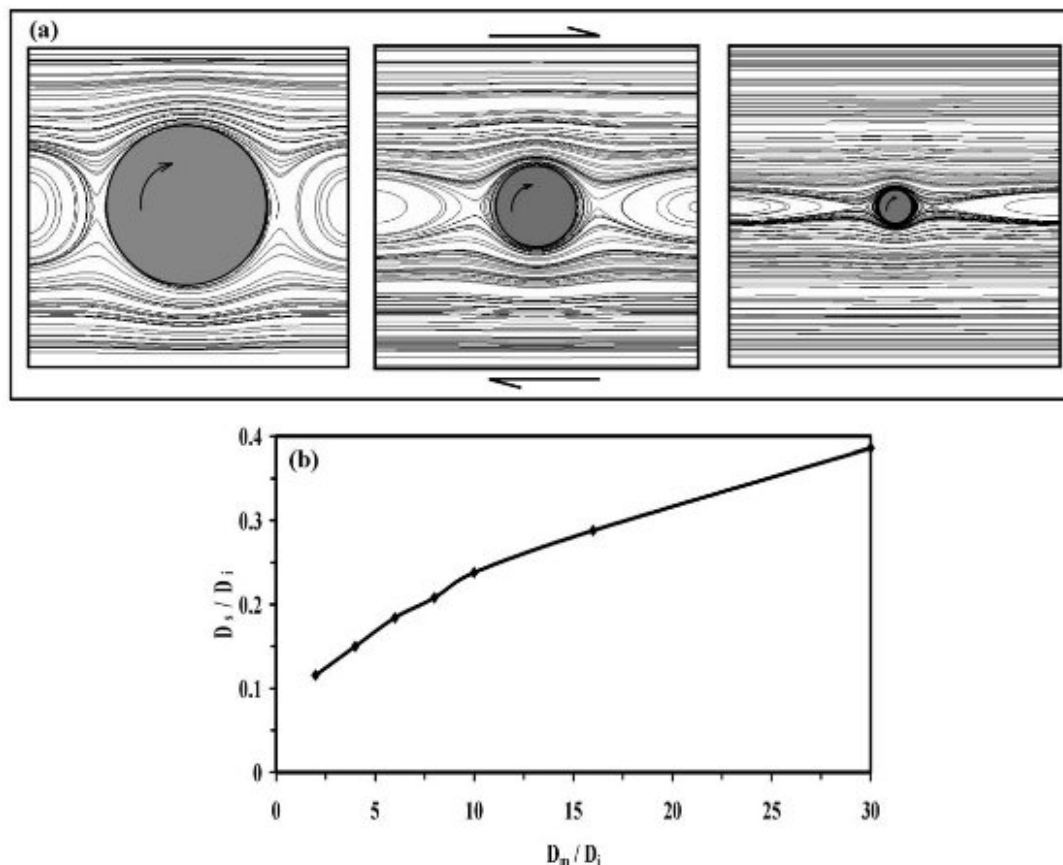
Fig. 6. (a) Flow patterns in models with varying inclusion/model dimension ratio (D_R). $D_R = 2$, 4 and 10 (left to right). Models were deformed by homogeneous shear displacement at the four boundaries of model, as done in shear box experiments (first condition shown in Fig. 5b). (b) Variation in the distance of stagnation points, normalized to D_i, with increasing model/inclusion dimension ratio (D_R).

However, eye-shaped flow becomes complex when the aspect ratio of model is increased to a critical value (e.g. $A_R = 2$). Two vortices form on either side of the inclusion, which are somewhat elliptical in shape (Fig. 8b). The model experiments suggest that FEM can give rise to a variety of flow patterns depending on the combination of dynamic settings at the model edges and the model geometry.

We ran a series of simulations imposing boundary conditions as adopted in physical experiments, where the model undergoes homogeneous shear with constrained lateral boundaries (*boundary condition-a*). Under this condition, flow with bow-tie shaped separatrix develop (Fig. 8c). The hyperbolic streamlines become narrow and the stagnation points move away from the inclusion with increasing model dimension (D_R), as shown in Section 3.3. Under this condition the flow pattern does not change with varying aspect ratio of models (Fig. 8d).

Under the straight-out conditions (Eqs. (10a) and (10b), *boundary condition-c*) models show contrasting types of flow patterns, depending on model aspect ratio, shown in Section 3.3. Models with low aspect ratio show eye-shaped flow pattern (e.g. Fig. 7a), which transforms into bow-tie shaped with increasing aspect ratio (e.g. Fig. 7b).

4. Discussion

Several inclusion-associated structures, e.g. porphyroclast tails, drag folds, are often used for kinematic analysis in shear zone rocks. Passchier and Simpson (1986) have shown elegantly how one can utilize σ- or δ-type porphyroclasts as shear sense indicator, considering their stair-stepped wings. The stair-stepping in wing geometry of δ-type porphyroclasts depends on the type of flow around the clasts (Passchier et al., 1993). For example, eye-shaped flow patterns are likely to produce wings on either side of the inclusion in the same plane, i.e. there is no stair-stepping. On the other hand, bow-tie shaped flow forms wings geometry with stair-stepping, which can be utilized for determination of the shear sense. Both stair-stepped and non-stair-stepped wings of porphyroclasts are observed in naturally deformed rocks. We therefore need to find possible physical factors determining the pattern of flow around a rigid inclusion.

The streamline patterns around spherical rigid inclusions are different in models of different workers, as discussed in Section 3.3. The difference essentially crops up due to consideration of models and the boundary settings imposed
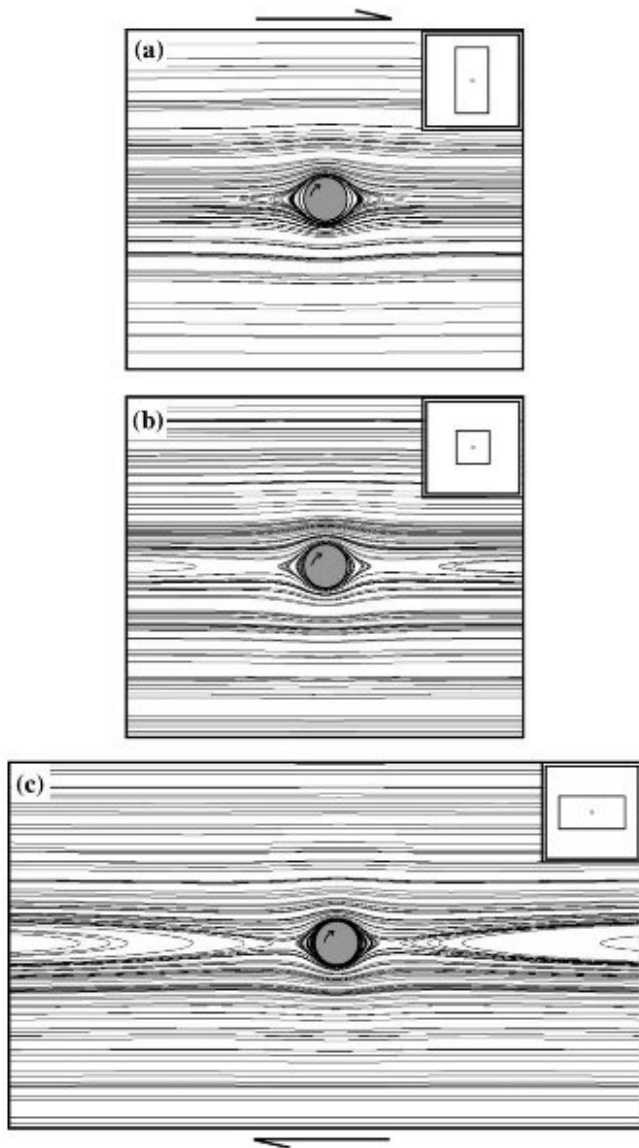
Fig. 7. Effect of model aspect ratio (A_R) on the flow pattern around rigid inclusion. Insets show initial models. $A_R = 0.5, 1, 2$ in (a)–(c). Models were deformed by homogeneous shear at the top and bottom boundaries, keeping a straight-out condition at the lateral boundaries (third boundary condition shown in Fig. 5b).

in the models (Bons et al., 1997). In the case of infinitely extended viscous matrix, the flow is described in terms of converging functions, which do not give rise to homogeneous flow field at any finite distance from the model. In such a condition, the perturbations imparted by the rigid body do not die out within a finite area (Masuda and Mizuno, 1996). On the other hand, physical modeling or finite element modeling involves boundary conditions imposed at a finite distance from the rigid body. For example, ideal simple shear conditions are imposed at the model edges, which are not likely to prevail at the same position had the matrix been considered as an infinitely extended medium. It may be noted that a slight pressure gradient far away from the inclusion can modify the flow

near the inclusion, which is somewhat similar to the butterfly effect in the theory of Chaos. This is the reason why FEMs show flow with bow-tie shaped separatrix, even when its dimensions are large compared with that of the inclusion. However, the effect of model dimension is evident from the increasing distance of stagnation points with increasing model dimension. The finding suggests that a bow-tie shaped flow with stagnation points located at infinite distances will resemble an eye-shaped flow (e.g. Marques et al., 2005).

Two stagnation points on either side of the inclusion characterize flow patterns with bow-tie shaped separatrix. We need to resolve the most fundamental question—can a particle have zero velocity in the flow field around an inclusion in systems under simple shear? In homogeneous simple shear all the particles on the central reference plane have zero velocity. They are set in motion with velocity component across the shear direction due to the perturbations induced by the rotational motion of rigid inclusions (Fig. 4d). The spatial occupancy of the sphere in the shear flow does not contribute any perturbations on this plane, which could result in velocity components across the shear direction. This is evident from the streamline pattern of flow around a stationary rigid sphere (fig. 31, Streeter, 1948). Now the perturbations in the flow due to the rotational motion of rigid inclusions are likely to prevail even at an infinite distance from the inclusion. It is thus evident that stagnation points are unlikely to exist in the flow field around a rigid body, as seen in Eqs. (8b) and (9b). In addition, in flows with bow-tie shaped separatrix, particles on the central reference plane flow in the opposite direction on either side of the stagnation points. It is rather difficult to explain the movement of particles across the central plane countering the rotational motion. It appears that this flow in the matrix is set in response to the pressure field generated due to the imposed motion set at the lateral boundaries of the model. To test this, we ran simulations of streamlines in the flow around a rigid body generated by rotating the lateral boundaries dextrally and keeping the other faces in the same positions. Such a boundary setting gives rise to hyperbolic paths cutting across the central reference plane (Fig. 9a). This type of flow is obtained even when the model dimension is very large compared with that of the inclusion. On the other hand, the plate motion parallel to the central reference plane on an unconstrained model gives close paths with velocity vectors acting opposite to that in the previous model (Fig. 9b). Now, if we impose one over another, at unique points the two velocity vectors cancel each other, giving rise to stagnation points, and the overall flow pattern resembles that of bow-tie shaped separatrix.

The FEMs described in Section 3.2 indicate that the flow geometry is a function of the model/inclusion dimension ratio, a parameter comparable with volume concentration of inclusion in the system. It has been shown that volume occupied by the inclusion in a FEM can greatly influence the flow of matrix around the inclusion (Treagus and Lan,
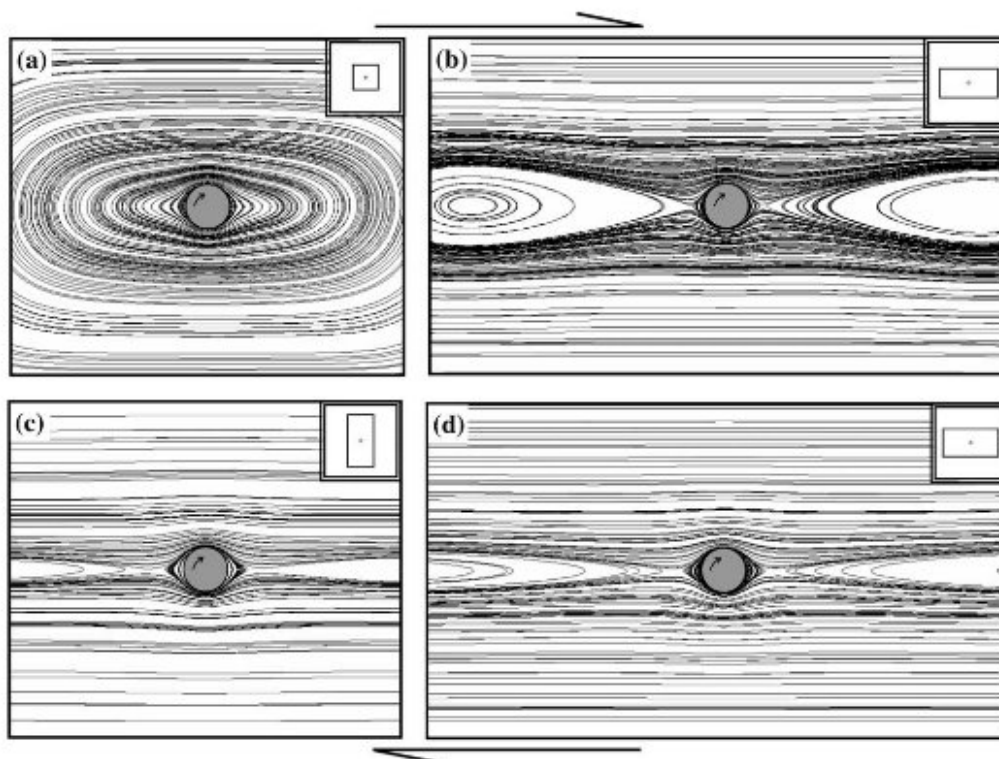
Fig. 8. (a) and (b) Flow patterns in square models and rectangular ($A_R = 2$) models with unconstrained lateral boundaries (second boundary condition shown in Fig. 5b). (c) and (d) Bow-tie shaped flow patterns in models of two different aspect ratios. $A_R = 0.5$ and 2. Homogeneous shear displacement (first condition shown in Fig. 5b) was set at the model boundaries.

2004). Samanta et al. (2003) presented an analysis of flow around a rigid inclusion as a function of volume concentration of inclusions. With decreasing concentration bow-tie shaped flow transforms into eye-shaped (Fig. 5; Samanta et al., 2003), which is consistent with the FEM results obtained by increasing model/inclusion dimension ratio (Fig. 6a). Flow with eye-separatrix should thus be considered in analyzing inclusion-associated structures in rocks containing inclusions in very low concentrations. Kinematics of flow with bow-tie shaped separatrix would be appropriate for systems with large inclusion concentrations, irrespective of shear zone width.

5. Conclusions

Based on our overview, we arrive at the following understandings. (1) The difference in observations on the flow patterns around rigid inclusions is essentially due to model constraints, as shown by Bons et al. (1997). Analytical solutions for the flow field suggest that the patterns will be essentially characterized by eye-shaped separatrix and that there cannot be any stagnation points in the flow around a rotating inclusion. (2) Flows with bow-tie shaped separatrix is likely to occur in finite inclusion–matrix systems, as reflected in the results of FEMs. When the model/inclusion dimension ratio is low, the separatrix defining the back flow regimes is nearly semi-circular,
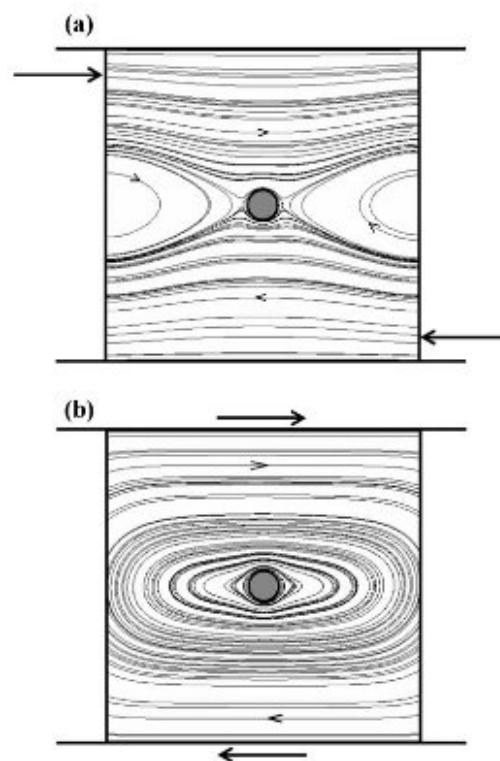

Fig. 9. (a) Flow induced by shear displacement on the lateral model boundaries. (b) Flow pattern developed in a model deformed by shear at the top and bottom boundaries, keeping the lateral boundaries unconstrained.

which progressively assumes an elliptical shape with increasing dimension ratio. In such cases the stagnation points continuously shift away from each other with increasing model/inclusion dimension ratio. (3) The flow pattern around a rigid inclusion can change dramatically depending on the boundary settings in the model. Unconstrained models in overall develop elliptical streamlines, and the flow in the neighborhood of inclusion show eye-shaped separatrix, whereas finite models with straight-out or homogeneous shear conditions of the boundary settings show flows with bow-tie shaped separatrix. (4) Under unconstrained state, eye-shaped flow turns into a flow with two vortices on either side of inclusion when the aspect ratio of model is large. (5) The use of flow patterns obtained from finite models should be made with care while interpreting natural structures in inclusion–matrix rock systems.

Acknowledgements

References

Bjornerud, M.G., Zhang, H., 1995. Flow mixing, inclusion-matrix coherence, mantle growth and the development of porphyroclast tails. Journal of Structural Geology 17, 1347–1350.

Bons, P.D., Barr, T.D., ten Brink, C.E., 1997. The development of δ-clasts in non-linear viscous materials: a numerical approach. Tectonophysics 270, 29–41.

Bose, S., Marques, F.O., 2004. Controls on the geometry of tails around rigid circular inclusions: insights from analogue modelling in simple shear. Journal of Structural Geology 26, 2145–2156.

Ghosh, S.K., Ramberg, H., 1976. Reorientation of inclusions by combination of pure shear and simple shear. Tectonophysics 34, 1–70.

Happel, J., 1957. Viscosity of suspensions of uniform spheres. Journal of Applied Physics 28, 1288–1292.

Jeffery, G.B., 1922. The motion of ellipsoidal particles immersed in a viscous fluid. Proceedings of the Royal Society of London A120, 161–179.

Jezek, J., Saic, S., Segeth, K., Schulmann, K., 1999. Three-dimensional hydrodynamical modelling of viscous flow around a rotating ellipsoidal inclusion. Computers and Geosciences 25, 547–558.

Lamb, H., 1932. Hydrodynamics. Cambridge University Press, Cambridge.

Mandal, N., Samanta, S.K., Chakraborty, C., 2000. Progressive development of mantle structures around elongate porphyroclasts: insights from numerical models. Journal of Structural Geology 22, 993–1008.

Mandal, N., Samanta, S.K., Chakraborty, C., 2001. Numerical modeling of heterogeneous flow fields around rigid objects with special reference to particle paths, strain shadows and foliation drag. Tectonophysics 330, 177–194.

Marques, F.O., Coelho, S., 2001. Rotation of rigid cylinders in viscous simple shear flow: analogue experiments. Journal of Structural Geology 23, 609–617.

Marques, F.O., Taborda, R., Bose, S., Antunes, J., 2005. Effects of confinement on matrix flow around a rigid inclusion in viscous simple shear: insights from analogue and numerical modelling. Journal of Structural Geology 27, 379–396.

Masuda, T., Ando, S., 1988. Viscous flow around a rigid spherical body: a hydrodynamical approach. Tectonophysics 148, 337–346.

Masuda, T., Mizuno, N., 1996. Deflection of non-Newtonian simple shear flow around a rigid cylindrical body by the finite element method. Journal of Structural Geology 18, 1089–1100.

Passchier, C.W., 1986. Stable positions of rigid objects in non-coaxial flow—a study in vorticity analysis. Journal of Structural geology 9, 679–690.

Passchier, C.W., 1994. Mixing in flow perturbations: a model for development of mantle porphyroclasts in mylonites. Journal of Structural Geology 16, 733–736.

Passchier, C.W., Simpson, C., 1986. Porphyroclast systems as kinematic indicators. Journal of Structural Geology 8, 831–844.

Passchier, C.W., Soukoutis, D., 1993. Experimental modelling of mantled porphyroclasts. Journal of Structural Geology 15, 895–909.

Passchier, C.W., ten Brink, C.E., Bons, P.D., Soukoutis, D., 1993. Delta objects as a gauge for stress sensitivity of strain rate in mylonites. Earth and Planetary Science Letters 120, 239–245.

Pennacchioni, G.P., Fasolo, L., Cecchi, M.M., Salasnich, L., 2000. Finite-element modeling of simple shear flow in Newtonian and non-Newtonian fluids around circular rigid particle. Journal of Structural Geology 22, 683–692.

Samanta, S.K., Mandal, N., Chakraborty, C., 2003. Flow patterns around rigid inclusions in a multiple inclusion system undergoing bulk simple shear deformation. Journal of Structural Geology 25, 209–221.

Streeter, V.L., 1948. Fluid Dynamics. McGraw-Hill Book Company, Inc, New York p. 263.

Taborda, R., Antunes, J., Marques, F.O., 2004. 2-D rotation behavior of a rigid ellipse in confined viscous simple shear: numerical experiments using FEM. Tectonophysics 379, 127–137.

ten Brink, C., Passchier, C.W., 1995. Modeling of mantled porphyroclasts using non-Newtonian rock analogue materials. Journal of Structural Geology 17, 131–146.

Treagus, S.H., Lan, L., 2004. Deformation of square objects and boudins. Journal of Structural Geology 26, 1361–1376.